Supplementary Information for

Decoupled Antarctic and Subarctic Export Productivity Under Intensified Southern Hemisphere Westerlies During the Last Interglacial

Lijuan Lu, Qinghua Yang*, Marcus Gutjahr, Qian Shi, Renhao Wu, Huang Huang, Yiming Luo, Hu Yang, Zhaoyang Song, Jiping Liu, Shuh-Ji Kao*

Corresponding authors: Q. Y. and S. K. (yangqh25@mail.sysu.edu.cn; sjkao@hainanu.edu.cn)

The PDF file includes:

Supplementary Figs. 1-13
Supplementary Tables 1-10
References

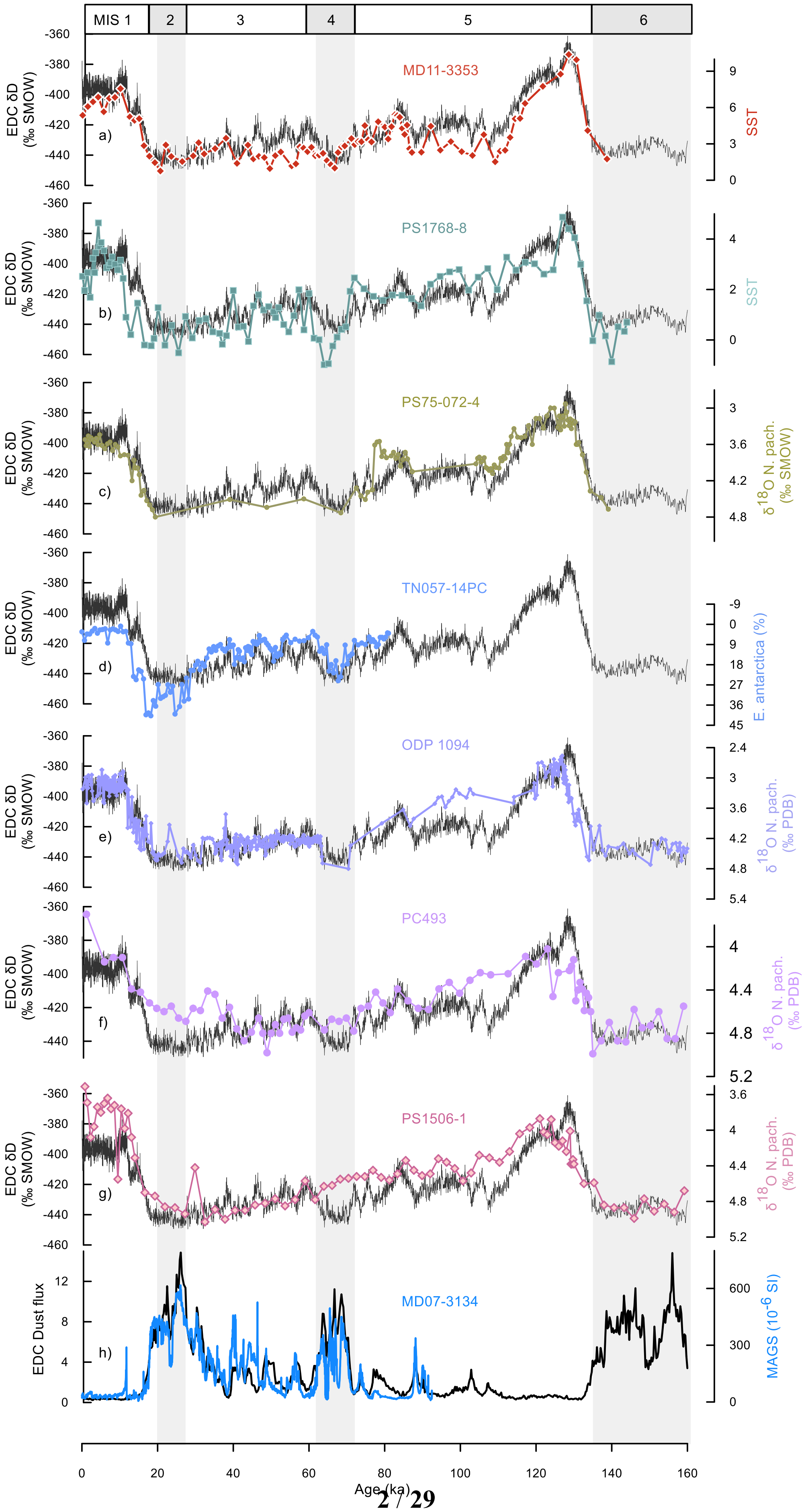

MIS 1
2
3
4
5
6
MD11-3353
PS1768-8
PS75-072-4
TN057-14PC
ODP 1094
PC493
PS1506-1
MD07-3134
EDC δD (‰ SMOW)
SST
δ18O N. pach. (‰ SMOW)
E. antarctica (%)
δ18O N. pach. (‰ PDB)
EDC Dust flux
MAGS (10-6 SI)
a)
b)
c)
d)
e)
f)
g)
h)
Age (ka)

Supplementary Fig. 1 | The refined age models for the compiled export productivity. a) EPICA DomeC (EDC) δD record[1,2] and MD11-3353 sea surface temperatures (SST)[3]. **b)** EDC δD record[1,2] and SST at Site PS1768-8[4]. **c)** EDC δD record[1,2] and planktonic foraminifera Neogloboquadrina pachyderma δ^{18}O at Site PS75-072-4[5]. **d)** EDC δD record[1,2] and the relative abundance of Eucampia antarctica at Site TN057-14PC[6]. **e)** EDC δD record[1,2] and planktonic foraminifera Neogloboquadrina pachyderma δ^{18}O at Site ODP 1094[7]. **f)** EDC δD record[1,2] and planktonic foraminifera Neogloboquadrina pachyderma δ^{18}O at Site PC493[8]. **g)** EDC δD record[1,2] and planktonic foraminifera Neogloboquadrina pachyderma δ^{18}O at Site PS1506-1[9]. **h)** EDC dust record[2,10] and magnetic susceptibility (MS) records at Site MD07-3134[11]. MIS=Marine Isotope Stage

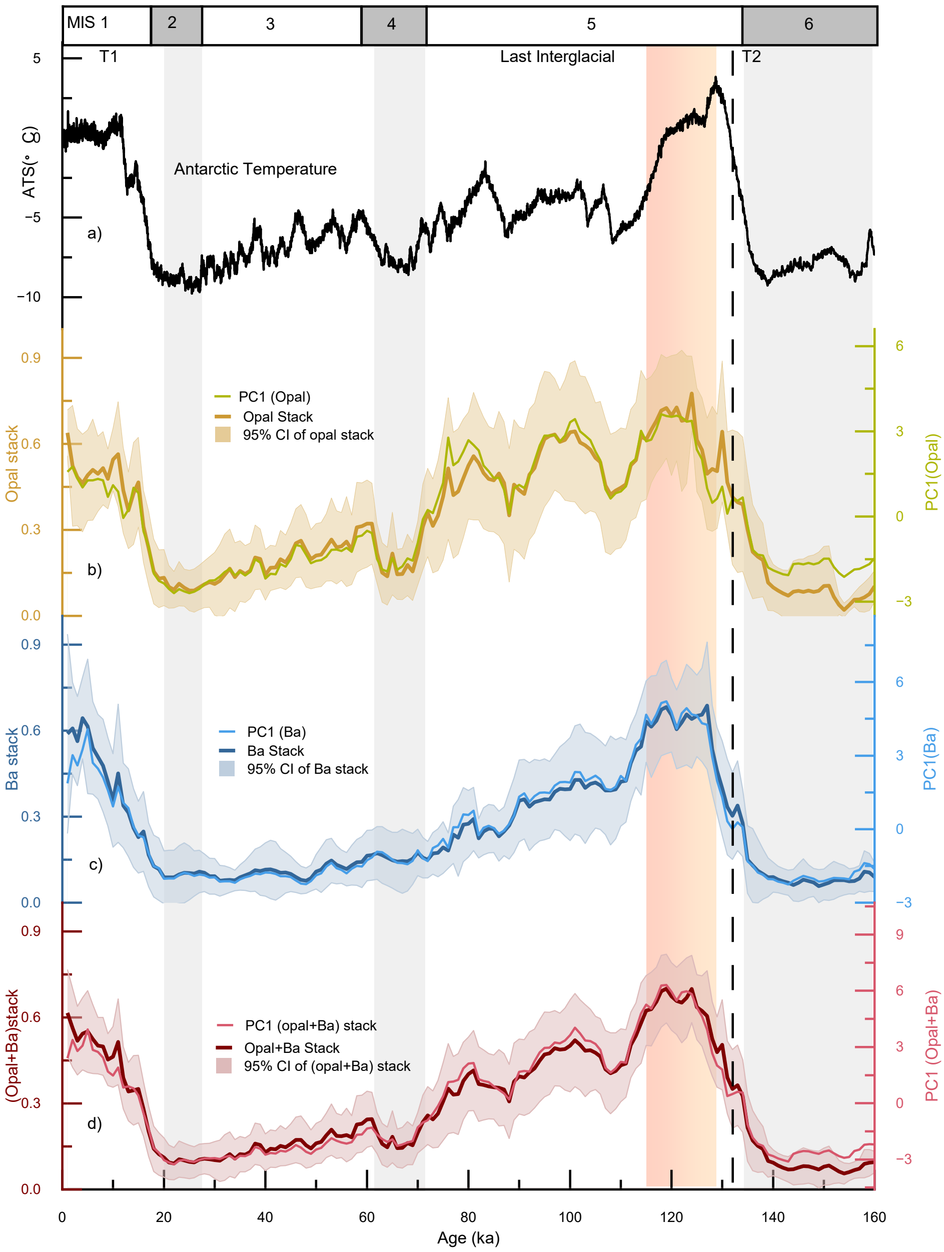

Supplementary Fig. 2 | Comparisons of different Antarctic export productivity (EP) stacks with the ATS. a) Antarctic air temperature stack (ATS)[12]. **b)** Biogenic opal stack (using the inverse standard deviation weighting method) and its confidence intervals (CI) of 95%, and scores of the first principal component (PC1) for related biogenic opal records (this study). **c)** Biogenic barium stack (using the inverse standard deviation weighting method) and its confidence intervals of 95%, and scores of PC1 for related biogenic barium records (this study). **d)** (biogenic opal+ biogenic barium) stack (using the inverse standard deviation weighting method) and its confidence intervals of 95%, and scores of PC1 for the combined biogenic opal and biogenic barium records (this study). MIS=Marine Isotope Stage

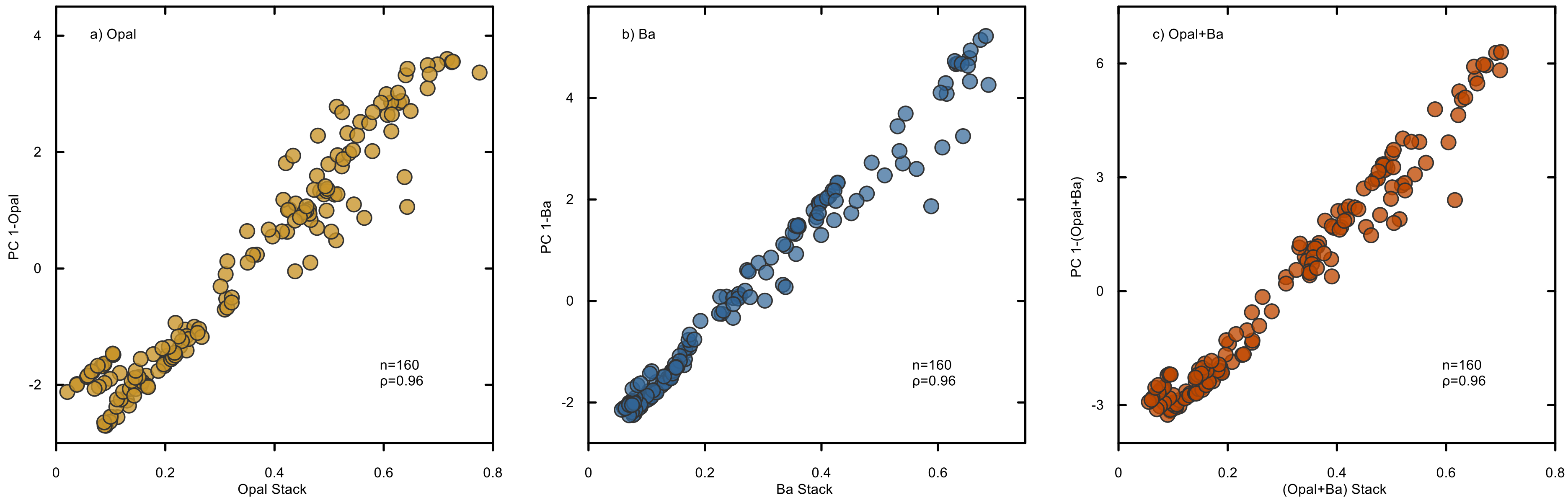

Supplementary Fig. 3 | Spearman's correlation of PC1 from the biogenic opal, biogenic barium, and combined (biogenic opal + biogenic barium) records with their respective stacks generated using the inverse standard deviation weighting method. a) Biogenic opal. **b)** Biogenic Ba. **c)** Combined (biogenic opal + biogenic barium). All correlations are significant at $p < 0.01$. Note: Spearman's correlation is used because the data are not normally distributed.

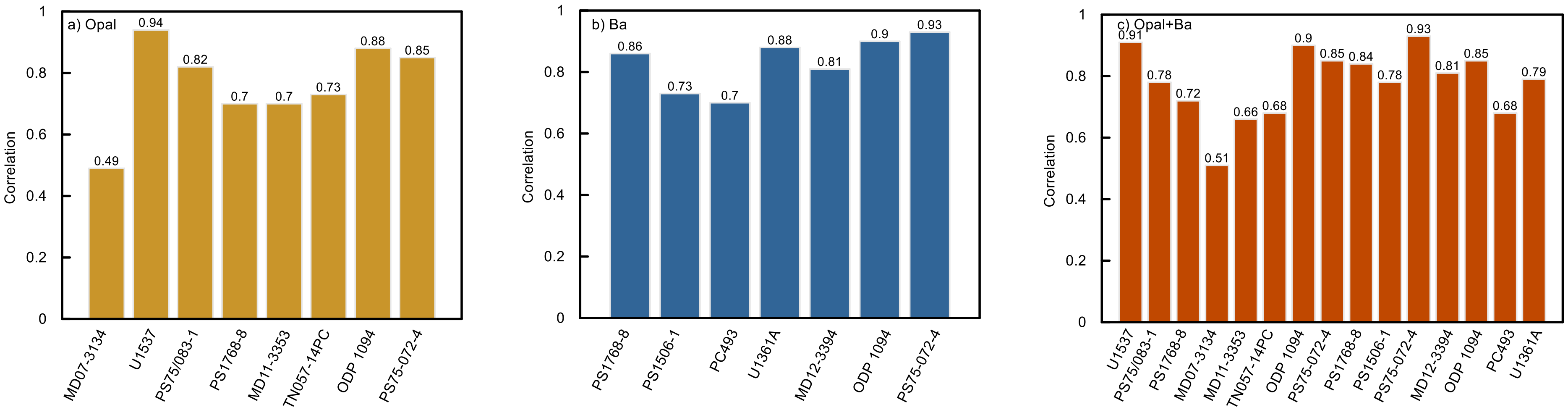

Supplementary Fig. 4 | Spearman's correlation between biogenic opal (a), barium (b), and the combined (biogenic opal + biogenic barium) records (c), calculated using the inverse standard deviation weighting method, with their corresponding records at different sites. All correlations are significant at $p < 0.01$. Note: Spearman's correlation is used because the data are not normally distributed. Strong correlations between each stack and its respective records support the significance of biogenic opal, biogenic Ba, and their combined stacks in capturing the underlying dynamics of Antarctic export productivity.

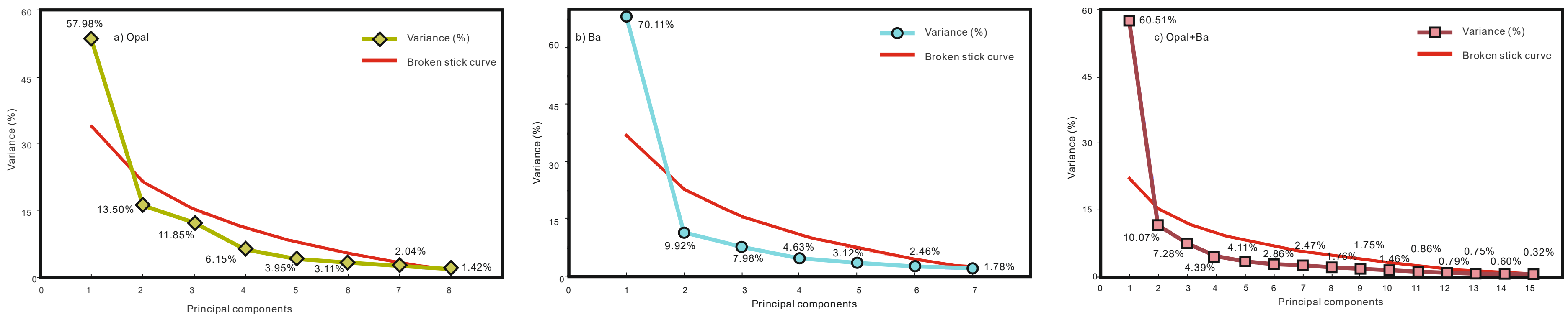

Supplementary Fig. 5 | The variance explained by each principal component of related Antarctic export productivity stacks, along with the broken stick curves (red). **a)** Biogenic opal. **b)** Biogenic barium. **c)** Combined (biogenic opal + biogenic barium). Red line represents the broken stick curve, which provides a reference for determining significant components. Principal components with variance above the red line are considered significant. All principal components except PC1 fall below the broken stick curve, indicating that only PC1 appears to carry enough signal for interpretation.

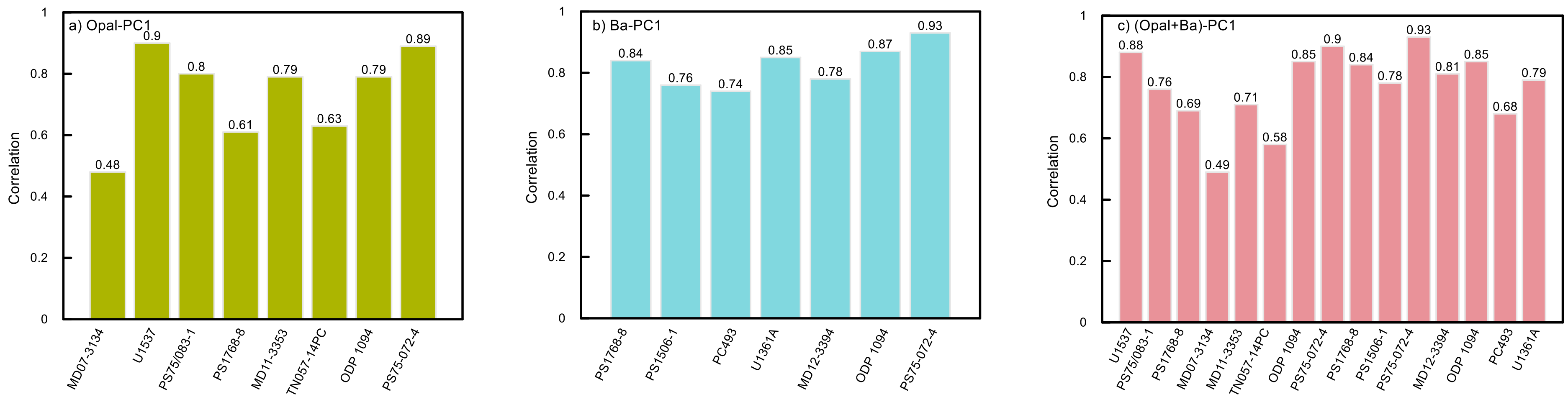

Supplementary Fig. 6 | Spearman's correlation of the related biogenic opal (a), barium (b), as well as the combined (biogenic opal + biogenic barium) records (c) on PC1, all of which are statistically significant ($p < 0.01$). The details of the related biogenic opal, biogenic barium, as well as combined (biogenic opal + biogenic barium) records are presented in Supplementary Table 1. Note: Spearman's correlation is used because the data are not normally distributed. Strong correlations between PC1 and the various variables support the significance of PC1 in capturing the underlying dynamics of the Antarctic export productivity.

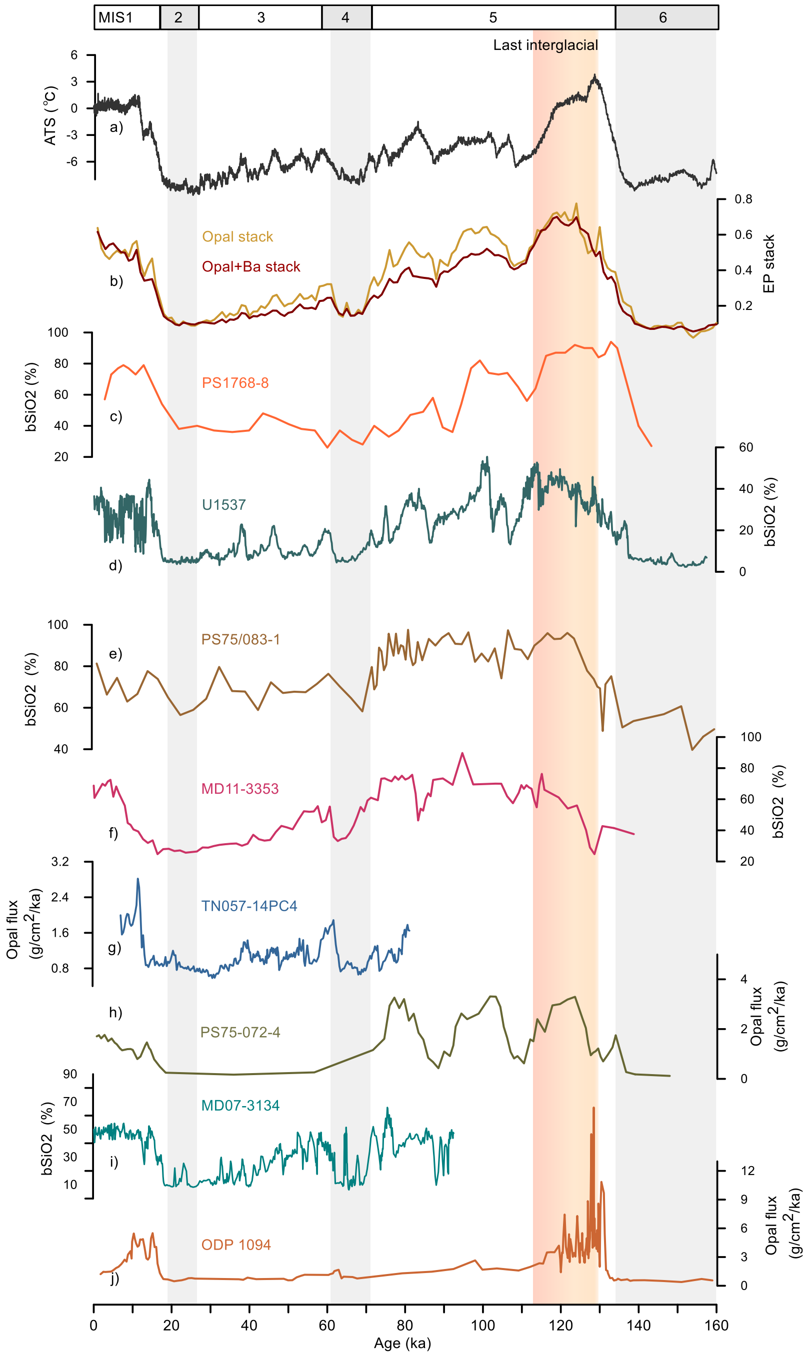

Supplementary Fig. 7 | Comparisons of opal and (opal+Ba) stack and the associated biogenic opal records in the Antarctic Zone of the Southern Ocean. a) Antarctic air temperature stack (ATS)[12]. **b)** Biogenic opal and (biogenic opal+ biogenic barium) stack (this study)**. c), d), e),** and **f)** are opal content at Site PS1768-8[4], U1537[13], PS75/083-1[14] and MD11-3353[3], respectively. **g)** and **h)** are the opal flux at Sites TN057-14PC4[6] and PS75-072-4[5], respectively. **i)** opal content at MD07-3134[15]. **j)** opal flux at Site ODP 1094[7]. MIS=Marine Isotope Stage

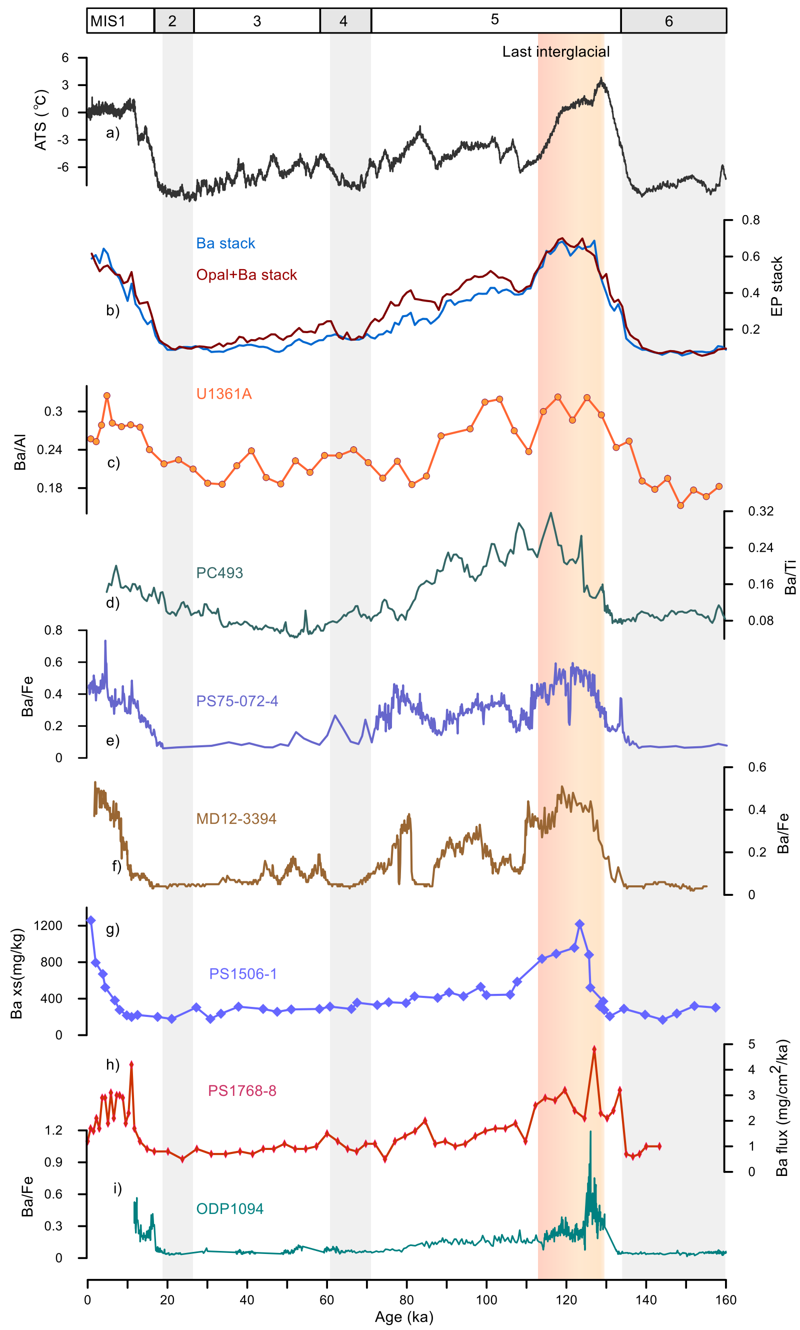

Supplementary Fig. 8 | Comparisons of biogenic barium and (opal+Ba) stack with the associated biogenic barium records in the Antarctic Zone of the Southern Ocean. a) Antarctic air temperature stack (ATS) [12]. **b)** biogenic barium and (biogenic opal+ biogenic barium) stack (this study)**. c)** Ba/Al at Site U1361A[16]. **d)** Ba/Ti at Site PC493[8]. **e)** and **f)** Ba/Fe at Sites PS75-072-4[5] and MD12-3394[18], respectively. **g)** and **h)** are the Ba concentrations at Sites PS1506-1[9] and PS1768-8[19], respectively. **i)** Ba/Fe at Sites ODP 1094[7]. MIS=Marine Isotope Stage

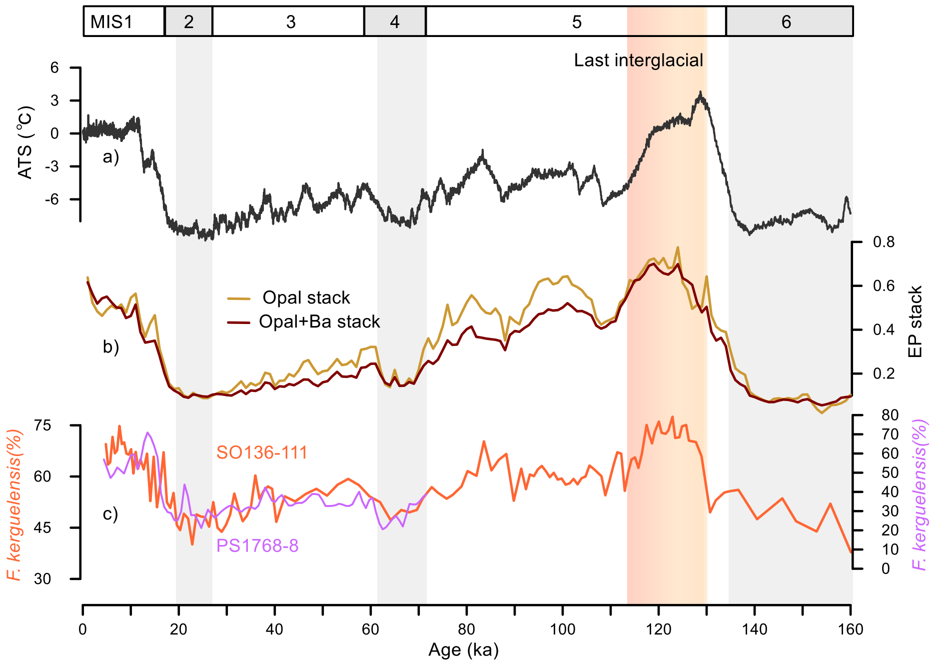

Supplementary Fig. 9 | Comparisons of Southern ocean export productivity (EP) stack, with the *Fragilariopsis kerguelensis* abundance records[20,21], a dominant diatom species in the permanent open ocean zone, and associated paleoclimate record. a) Antarctic air temperature stack (ATS)[12]; **b)** EP as inferred from opal stack and (opal+ barium) stack (this study); **c)** The relative abundance of *Fragilariopsis kerguelensis* records[20,21] in the permanent open ocean zone of Antarcitc zone of Southern Ocean. MIS=Marine Isotope Stage

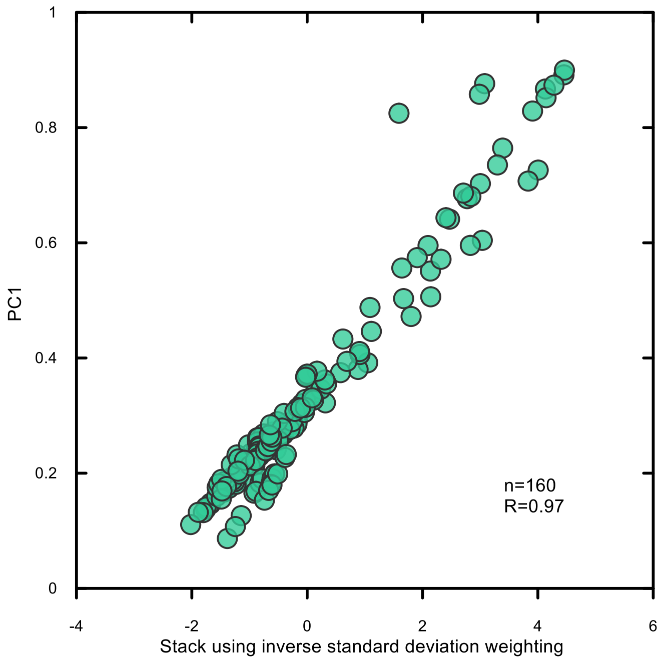

Supplementary Fig. 10 | Correlation of PC1 with Subarctic Pacific export productivity stack using the inverse standard deviation weighting method (significant at $p < 0.01$). Note: Pearson's correlation was used because the data were approximately normally distributed.

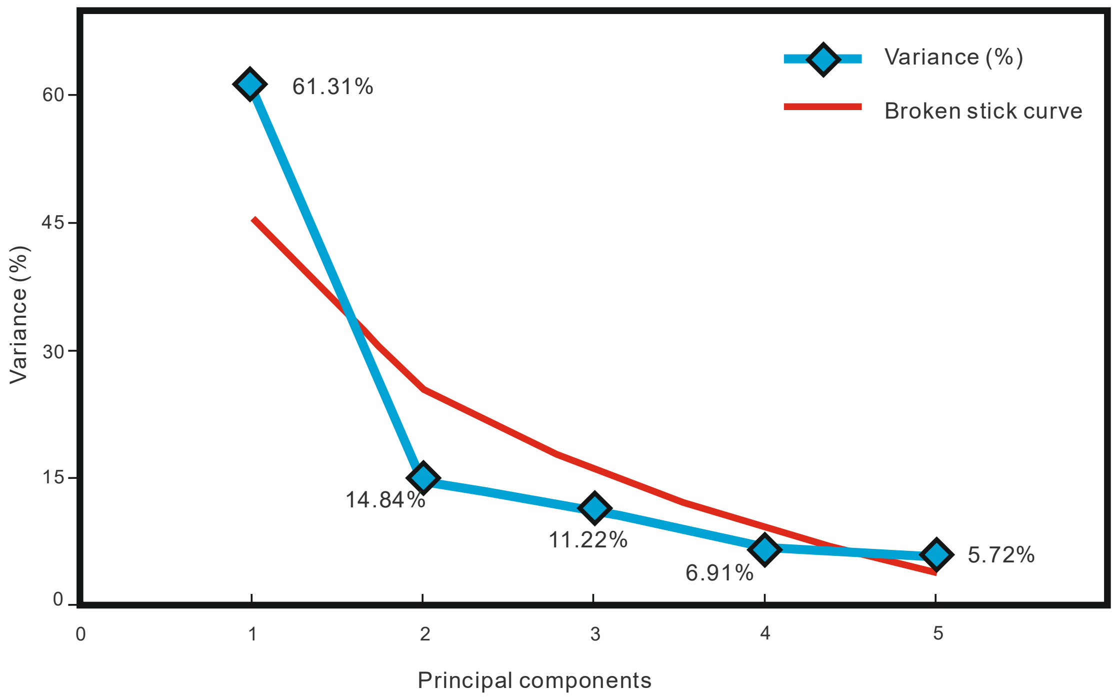

Supplementary Fig. 11 | The variance explained by each principal component for Subarctic Pacific export productivity stack, along with the broken stick curve. The blue line with diamond shows the variance explained by each principal component. Red line represents the broken stick curve, which provides a reference for determining significant components. Principal components with variance above the red line are considered significant.

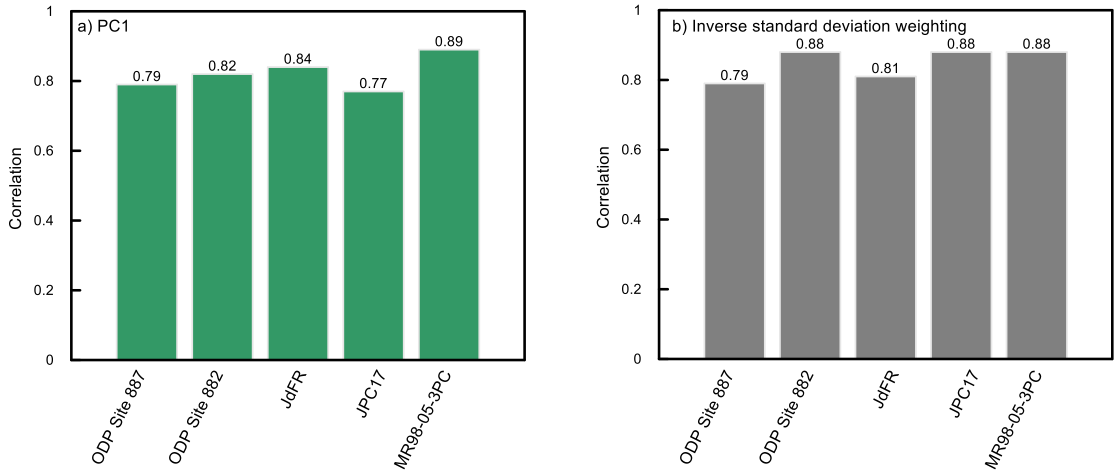

Supplementary Fig. 12 | Pearson's correlations of subarctic Pacific export productivity records with (a) PC1 and (b) the export productivity stack derived using the inverse standard deviation weighting method (all correlations significant at $p < 0.01$). Note: Pearson's correlation was used because the data were approximately normally distributed.

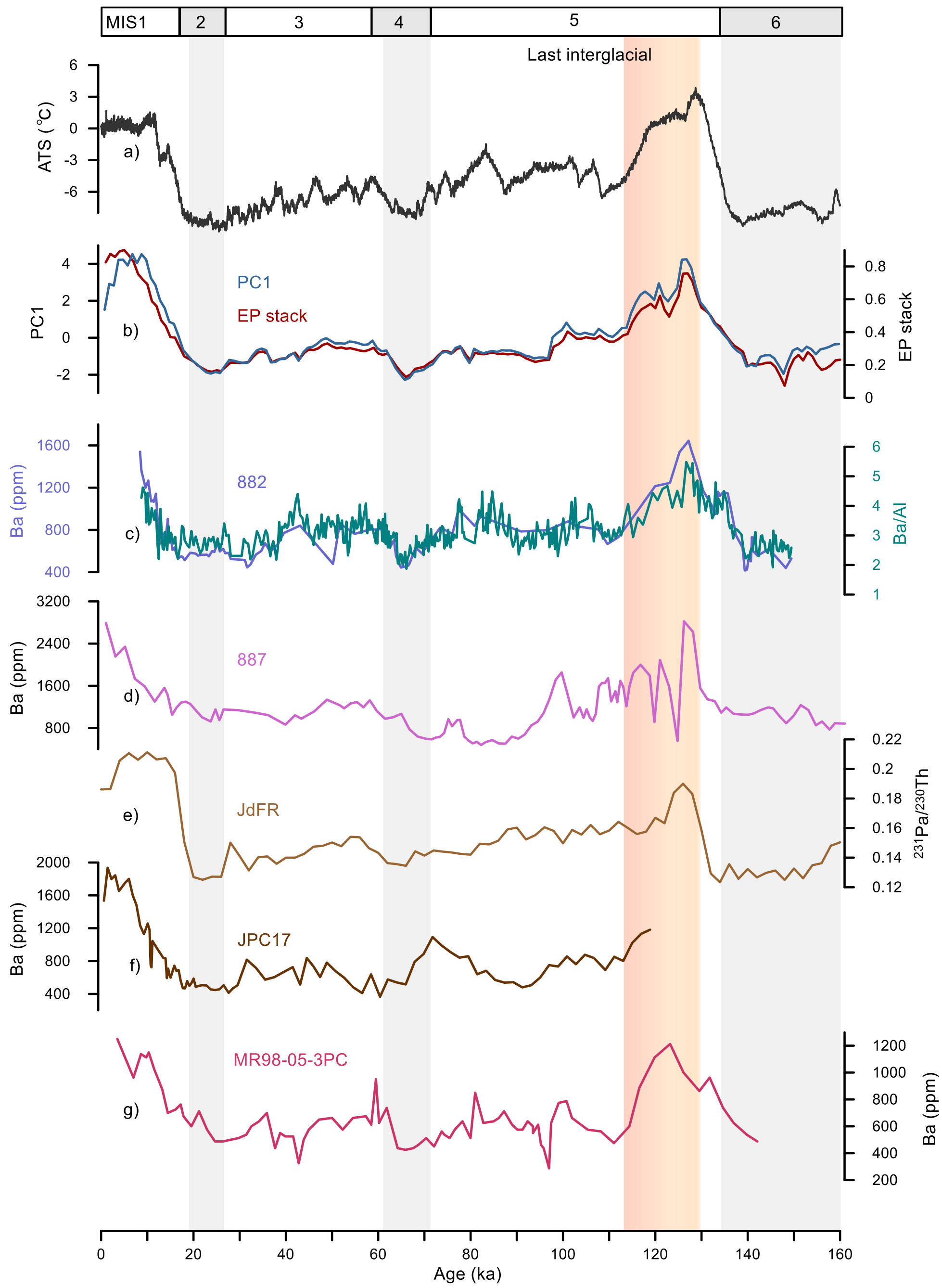

Supplementary Fig. 13 | Comparisons of the Subarctic Pacific export productivity stacks with related records. a) Antarctic air temperature stack (ATS)[12]. **b)** Subarctic Pacific export productivity stack using the inverse standard deviation weighting method and the PC1 of the related Subarctic Pacific export productivity records. **c)** Biogenic barium concentration and Ba/Al at ODP Site 882[22,23]. **d)** Biogenic barium concentration at ODP Site 887[24]. **e)** $^{231}Pa/^{230}Th$ stack from the Juan de Fuca Ridge (JdFR)[25]. **f)** Biogenic barium concentration at JPC17[26]. **g)** Biogenic barium concentration at MR98-05-3PC[27]. MIS=Marine Isotope Stage

Supplementary Table 1 | Details for sediment cores for reconstructing the EP stack in the Antarctic Zone of the Southern Ocean.

Number	Sites	Depth (m)	Latitude	Longitude	Proxy	Age scale (ka)	Chronology	Age scale	Opal stack	Ba stack	(Opal+Ba) stack	Reference
1	MD11-3353	1568	-50.57	68.39	$bSiO_2$ [%]	138.7-0	TEX_{86}^{L}-SST - EDC δD	adjusted to AICC2012	√		√	Thöle et al., 2019[3]
2	PS1768-8	3299	-53.6	4.5	$bSiO_2$ [%]	143-2.5	SST- EDC δD	adjusted to AICC2012	√		√	Frank et al., 2000[4]
3	MD07-3134	3663	-59.41	-41.47	$bSiO_2$ [%]	92.5-0	MS - EDML $nssCa^{2+}$ flux	adjusted to AICC2012	√		√	Sprenk et al., 2013[15]
4	U1537	3713	-59.1	-40.9	$bSiO_2$ [%]	160.1-0.2	MS - EDC dust	AICC2012	√		√	Lu et al., 2022[13]
5	PS75/083-1	3599	-60.27	-159.06	$bSiO_2$ [%]	162.2-0.8	Fe - EDC dust	AICC2012	√		√	Lamy et al., 2024[14]
6	PS75-072-4	3099	-57.56	-151.22	Opal flux	148.0-0.8	^{14}C; $\delta^{18}O$ - EDC δD	adjusted to AICC2012	√		√	Studer et al., 2015[5]
7	TN057-14PC	3648	-51.98	4.5	Opal flux	80.8-6.6	Benthic $\delta^{18}O$ - MD95-2042	adjusted to AICC2012	√		√	Anderson, et al, 2009[6]
8	ODP 1094	2850	-52.2	5.1	Opal flux	160.2-1.5	Planktonic δ18O - EDC δD	adjusted to AICC2012	√		√	Jaccard et al., 2013[7]
9	MD12-3394	2320	-48.38	64.58	Ba/Fe	155.2-1.6	^{14}C; TEX86L- SST to ATS	AICC2012		√	√	Ai et al., 2020[18]
10	U1361A	3454	-64.41	143.89	Ba/Al	162.0-1.3	Ba/Al -EDC δD	AICC2012		√	√	Wilson et al., 2018[16,17]
11	PS75-072-4	3099	-57.56	-151.22	Ba/Fe	160.7-0.8	^{14}C; $\delta^{18}O$ - EDC δD	adjusted to AICC2012		√	√	Studer et al., 2015[5]
12	PC493	2077	-71.13	-119.91	Ba/Ti	160.3-4.8	$\delta^{18}O$ N. pach. sin. or $\delta^{18}O$ Cib.- EDC δD	adjusted to AICC2012		√	√	Williams et al., 2019[8]
13	PS1506-1	2426	-68.73	-5.85	Ba_{xs}	161.8-0.8	N. pachyderma $\delta^{18}O$-EDC δD	adjusted to AICC2012		√	√	Shimmield et al., 1994[9]
14	PS1768-8	3299	-53.6	4.5	Ba_{ex} flux	143.3-0	SST- EDC δD	adjusted to AICC2012		√	√	Nürnberg et al., 1997[19]
15	ODP 1094	2850	-52.2	5.1	Ba/Fe	160-11.7	Planktonic $\delta^{18}O$ - EDC δD	adjusted to AICC2012		√	√	Jaccard et al., 2013[7]

Supplementary Table 2 | Details for sediment cores for reconstructing the expert productivity stack in the subarctic Pacific

Number	Sites	Depth (m)	Latitude	Longitude	Proxy	Age scale (ka)	Chronology	Reference
1	ODP882	3244	50.33	167.58	Biogenic Ba	149.7-8.6	Magnetostratigraphy; tuning of GRAPE density (precession band) to 65°N summer insolation; inter-site alignment of benthic $\delta^{18}O$ (Sites 882 & 883) within $CaCO_3$-bearing intervals, corroborated by magnetic susceptibility; fine-tuning of BioBa record (Site 882) to Vostok δD	Jaccard et al., 2005[22]
2	ODP887	3647	54.22	-148.27	Biogenic Ba	161-1	AMS ^{14}C; survey core-887B stratigraphic and geochemical correlation; $\delta^{18}O$ correlation to SPECMAP	McDonald et al., 1999[24]
3	MR98-05-3PC	5507	50.00	164.98	Biogenic Ba	142-3.5	Normalized remanence intensity vs paleointensity curve; AMS ^{14}C; Opal content correlation to nearby core RAMA44PC	Fukuma and Harada, 2001[28]; Shigemitsu et al., 2007[27]
4	JPC17	2209	53.93	178.90	Biogenic Ba	118.8-0.6	AMS ^{14}C; Planktonic and benthic $\delta^{18}O$	Brunelle et al., 2007[26]
5	Juan de Fuca Ridge (JdFR) stack	2794	44.96	-130.65	$^{231}Pa/^{230}Th$	160-0	AMS ^{14}C; benthic $\delta^{18}O$; stratigraphically tuned density cycles	Costa et al., 2016[29], 2018[25]

Note that the Juan de Fuca Ridge (JdFR) $^{231}Pa/^{230}Th$ stack is a regional average of Sites AT26-19-05PC (44.97°N, -130.88°E), 09PC/06MC (44.89°N, -130.64°E), 12PC-TC/10MC(44.89°N, -130.50°E), 35PC (44.99°N, -130.46°E), 38PC (44.97°N, -130.61°E), and 39BB (45.05°N, -130.83°E), as the glacial-interglacial trends in these six cores are sufficiently similar to be combined into a single stack[25].

Supplementary Table 3 | Age model for Site MD11-3353.

Tie Point	Depth (m)	AICC 2012	AICCAge std dev [±]	Chronology constraint method
1	0.1	0.200000034	0.101475417	SST to EDC δD record
2	0.7	4.299997032	0.207130974	SST to EDC δD record
3	1.5	10.19994901	0.26507645	SST to EDC δD record
4	1.994	16.30005792	0.643383712	SST to EDC δD record
5	4.718	55.70001722	0.901485158	SST to EDC δD record
6	5.8	66.80003378	2.343476341	SST to EDC δD record
7	7.6	82.70001638	1.554271186	SST to EDC δD record
8	8.3	87.2	1.661168449	SST to EDC δD record
9	8.62	95.20003476	1.594998917	SST to EDC δD record
10	8.9	103.2002222	1.684508889	SST to EDC δD record
11	9.3	109.2	1.753563333	SST to EDC δD record
12	10.5	117.1001844	1.651495177	SST to EDC δD record
13	10.901	126.5000598	1.774039573	SST to EDC δD record
14	11.083	128.3	1.725388333	SST to EDC δD record
15	11.27	132.1	1.993792642	SST to EDC δD record
16	11.403	138.9	2.743373107	SST to EDC δD record

Supplementary Table 4 | Age model for Site PS1768-8

Tie Point	Depth (m)	AICC 2012	AICCAge std dev [±]	Chronology constraint method
1	0	0	0.078589358	SST to EDC δD record
2	1.65	12	0.334631244	SST to EDC δD record
3	3.2	40	0.667879148	SST to EDC δD record
4	5	64	2.45093465	SST to EDC δD record
5	5.7	72	1.682480579	SST to EDC δD record
6	7.25	111	1.735842093	SST to EDC δD record
7	7.9	127	1.7834024	SST to EDC δD record
8	8.4	135	2.420344	SST to EDC δD record
9	9	145	2.892528127	SST to EDC δD record

Supplementary Table 5 | Age model for Site MD07-3134.

Tie Point	Depth (m)	AICC 2012	AICCAge std dev [±]	Chronology constraint method
1	0	0	0	MS to EDML nssCa2＋flux
2	8.91	11.74	0.288322	MS-EDC dust
3	15.52	18.386	0.945289	MS to EDML nssCa2＋flux
4	15.77	19.12	0.970847	MS to EDML nssCa2＋flux
5	16	20.064	0.914693	MS to EDML nssCa2＋flux
6	16.37	21.189	1.104071	MS to EDML nssCa2＋flux
7	16.76	22.46	1.003432	MS-EDC dust
8	16.95	23.802	0.979002	MS-EDC dust
9	17.81	26.12	0.985762	MS-EDC dust
10	18.33	28.64	0.809323	MS-EDC dust
11	18.82	30.36	0.966088	MS-EDC dust
12	20.4	32.83	0.8135	MS to EDML nssCa2＋flux
13	22.59	35.76	0.835463	MS to EDML nssCa2＋flux
14	24.7	38.459	0.599395	MS to EDML nssCa2＋flux
15	25.08	39.23	0.591414	MS to EDML nssCa2＋flux
16	26.19	41.646	0.702241	MS to EDML nssCa2＋flux
17	26.31	42.05	0.747251	MS to EDML nssCa2＋flux
18	26.65	42.98	0.792201	MS to EDML nssCa2＋flux
19	26.97	44.27	0.749737	MS to EDML nssCa2＋flux
20	27.49	46.39	0.751533	MS to EDML nssCa2＋flux
21	28.38	47.657	0.895749	MS to EDML nssCa2＋flux
22	29.35	48.67	1.019878	MS to EDML nssCa2＋flux
23	33.38	54.17	0.810662	MS to EDML nssCa2＋flux
24	33.95	55.69	0.903069	MS to EDML nssCa2＋flux
25	34.08	56.65	0.97938	MS-EDC dust
26	38.66	60.5	1.282327	MS to EDML nssCa2＋flux
27	40.06	62.071	1.450498	MS to EDML nssCa2＋flux
28	40.52	63.62	2.320324	MS-EDC dust
29	43.2	65.52	1.621985	MS to EDML nssCa2＋flux
30	44.05	66.349	1.644043	MS to EDML nssCa2＋flux
31	44.92	67.061	1.660484	MS to EDML nssCa2＋flux
32	45.41	68.58	1.939747	MS-EDC dust
33	46.45	71.81	1.681406	MS-EDC dust
34	46.91	73.56	2.075441	MS-EDC dust
35	50.37	77.07	1.795199	MS-EDC dust
36	54.2	87.86	1.728806	MS-EDC dust
37	55.23	90.64	1.592727	MS-EDC dust
38	58.06	92.49	1.506477	MS to EDML nssCa2＋flux

Supplementary Table 6 | Age model for Site PS75-072-4.

Tie Point	Depth (m)	AICC 2012	AICCAge std dev [±]	Chronology constraint method
1	0.02	0.838612	0.131957	14C
2	0.22	2.0088	0.149987	14C
3	0.52	4.708529	0.219131	14C
4	0.92	10.27867	0.257843	14C
5	1.073	13.31127	0.452924	d18O to EDC dD
6	1.32	16.10538	0.57601	14C
7	1.572	19.42081	0.954503	d18O to EDC dD
8	1.615	38.09287	0.580083	d18O to EDC dD
9	1.771	68.60623	1.936487	d18O to EDC dD
10	1.819	72.47341	1.766247	d18O to EDC dD
11	1.92	74.88667	1.854567	d18O to EDC dD
12	2.95	87.66899	1.748037	d18O to EDC dD
13	4.056	103.9899	1.748599	d18O to EDC dD
14	4.702	109.672	1.73003	d18O to EDC dD
15	5.191	113.6011	1.696797	d18O to EDC dD
16	5.826	125.8997	1.79248	d18O to EDC dD
17	6.671	131.2547	1.877435	d18O to EDC dD
18	6.875	135.432	2.429248	d18O to EDC dD
19	6.98	139.487	2.768286	d18O to EDC dD
20	7.201	188.7781	2.529094	Ba/Fe
21	7.381	192.8726	2.340938	Diatom LOD H. karstenii
22	7.543	199.2934	1.964873	d18O to EDC dD
23	8.299	206.7791	2.139612	d18O to EDC dD
24	9.207	220.9046	2.750496	d18O to EDC dD

Supplementary Table 7. Age model for Site TN057-14PC.

Tie Point	Depth (cm)	AICC 2012	AICCAge std dev [±]	Chronology constraint method
1	0	0	0	/
2	220	15	0.451627	Eucampia antarctica record -EDC
3	360	24	1.058379	Eucampia antarctica record -EDC
4	610	39	0.613311	Eucampia antarctica record -EDC
5	850	46.86	0.831775	Eucampia antarctica record -EDC
6	1000	54	0.813656	Eucampia antarctica record -EDC
7	1060	61	1.973826	Eucampia antarctica record -EDC
8	1240	72	1.682481	Eucampia antarctica record -EDC
9	1280	75.88	1.803869	Eucampia antarctica record -EDC
10	1385	81	1.532061	Eucampia antarctica record -EDC

Supplementary Table 8 | Age model for Site ODP 1094.

Tie Point	Depth (m)	AICC 2012	AICCAge std dev [±]	Chronology constraint method
1	0	0.205459	0.101848	d18O to EDC dD
2	3.74	6.851414	0.229054	d18O to EDC dD
3	6.42	11.8798	0.315074	d18O to EDC dD
4	8.61	20.05451	0.939913	d18O to EDC dD
5	9.5	28.29825	0.703662	d18O to EDC dD
6	10.04	35.0453	0.88974	d18O to EDC dD
7	17.79	63.6702	2.34638	d18O to EDC dD
8	18.44	71.22213	1.901205	d18O to EDC dD
9	18.91	84.69416	1.744785	d18O to EDC dD
10	20.46	113.5099	1.699091	d18O to EDC dD
11	24.45	126.4737	1.772235	d18O to EDC dD
12	26.21	130.1749	1.790881	d18O to EDC dD
13	26.95	134.2283	2.256126	d18O to EDC dD
14	27.99	150.71	3.567286	d18O to EDC dD
15	28.19	154.819	3.844825	d18O to EDC dD
16	28.52	158.3066	3.691286	d18O to EDC dD
17	29.23	161.9433	3.522903	d18O to EDC dD

Supplementary Table 9 | Age model for Site Site PC493.

Tie Point	Depth (m)	AICC 2012	AICCAge std dev [±]	Chronology constraint method
1	0	0	0	d18O to EDC dD
2	7.5	17.85	0.888828861	d18O to EDC dD
3	22.5	46.69	0.780305473	d18O to EDC dD
4	34.5	60	1.222652177	d18O to EDC dD
5	35.5	64.07	2.435159401	d18O to EDC dD
6	45.5	83.41	1.582095672	d18O to EDC dD
7	54.5	108	1.836801902	d18O to EDC dD
8	56.5	117.22	1.650136617	d18O to EDC dD
9	60.5	128.81	1.725040541	d18O to EDC dD
10	71.5	135	2.420344	d18O to EDC dD
11	86.5	167.7	3.013170588	d18O to EDC dD
12	87.5	169.9	3.022165676	d18O to EDC dD
13	93.5	180.89	2.571741115	d18O to EDC dD

Supplementary Table 10 | Age model for Site PS1506-1.

Tie Point	Depth (m)	AICC 2012	AICCAge std dev [±]	Chronology constraint method
1	0	0.5	0.120202545	d18O to EDC dD
2	0.45	14	0.469285808	d18O to EDC dD
3	1	62.5	2.158804787	d18O to EDC dD
4	1.59	105	1.784178385	d18O to EDC dD
5	1.77	121	1.662474882	d18O to EDC dD
6	2.01	129	1.734211132	d18O to EDC dD
7	2.13	130	1.776080504	d18O to EDC dD
8	2.82	191	2.424148111	d18O to EDC dD

References

1. Jouzel, J., Masson-Delmotte, V., Cattani, O., Dreyfus, G., Falourd, S., Hoffmann, G., ... & Wolff, E. W. Orbital and millennial Antarctic climate variability over the past 800,000 years. *Science* **317**, 793-796 (2007).
2. Bazin, L., Landais, A., Lemieux-Dudon, B., Toyé Mahamadou Kele, H., Veres, D., Parrenin, F., ... & Wolff, E. An optimized multi-proxy, multi-site Antarctic ice and gas orbital chronology (AICC2012): 120–800 ka. *J. Clim.* **9**, 1715-1731 (2013).
3. Thöle, L. M., Amsler, H. E., Moretti, S., Auderset, A., Gilgannon, J., Lippold, J., ... & Jaccard, S. L. Glacial-interglacial dust and export production records from the Southern Indian Ocean. *Earth Planet Sc. Lett.* **525**, 115716 (2019).
4. Frank, M., Gersonde, R., van der Loeff, M. R., Bohrmann, G., Nürnberg, C. C., Kubik, P. W., ... & Mangini, A. Similar glacial and interglacial export bioproductivity in the Atlantic sector of the Southern Ocean: Multiproxy evidence and implications for glacial atmospheric CO_2. *Paleoceanography* **15**, 642-658 (2000).
5. Studer, A. S., Sigman, D. M., Martínez-García, A., Benz, V., Winckler, G., Kuhn, G., ... & Haug, G. H. Antarctic Zone nutrient conditions during the last two glacial cycles. *Paleoceanography* **30**, 845-862 (2015).
6. Anderson, R. F., Ali, S., Bradtmiller, L. I., Nielsen, S. H. H., Fleisher, M. Q., Anderson, B. E., & Burckle, L. H. Wind-driven upwelling in the Southern Ocean and the deglacial rise in atmospheric CO_2. *Science* **323**, 1443-1448 (2009).
7. Jaccard, S. L., Hayes, C. T., Martinez-Garcia, A., Hodell, D. A., Anderson, R. F., Sigman, D. M., Haug, G. H. Two modes of change in Southern Ocean productivity over the past million years. *Science* **339**, 1419-1423 (2013).
8. Williams, T. J., Hillenbrand, C. D., Piotrowski, A. M., Allen, C. S., Frederichs, T., Smith, J. A., ... & Hodell, D. A. Paleocirculation and ventilation history of Southern Ocean sourced deep water masses during the last 800,000 years. *Paleoceanogr. Paleoclimatol.* **34**, 833-852 (2019).
9. Shimmield, G., Derrick, S., Mackensen, A., Grobe, H., & Pudsey, C. The history of barium, biogenic silica and organic carbon accumulation in the Weddell Sea and Antarctic Ocean over the last 150,000 years. In *Carbon Cycling in the Glacial Ocean: Constraints on the Ocean's*

Role in Global Change: Quantitative Approaches in Paleoceanography (pp. 555-574). Springer Berlin Heidelberg (1994).

10. Lambert, F., Bigler, M., Steffensen, J. P., Hutterli, M., & Fischer, H. Centennial mineral dust variability in high-resolution ice core data from Dome C, Antarctica. *Clim. Past* **8**, 609-623 (2012).
11. Weber, M. E., Kuhn, G., Sprenk, D., Rolf, C., Ohlwein, C., & Ricken, W. Dust transport from Patagonia to Antarctica–a new stratigraphic approach from the Scotia Sea and its implications for the last glacial cycle. *Quat. Sci. Rev.* **36**, 177-188 (2012).
12. Parrenin, F., Masson-Delmotte, V., Köhler, P., Raynaud, D., Paillard, D., Schwander, J., ... & Jouzel, J. Synchronous change of atmospheric CO_2 and Antarctic temperature during the last deglacial warming. *Science* **339**, 1060-1063 (2013).
13. Lu, L., Zheng, X., Chen, Z., Yan, W., Wu, S., Zheng, L. W., ... & Kao, S. One-To-One Coupling Between Southern Ocean Productivity and Antarctica Climate. *Geophys. Res. Lett.* **49**, e2022GL098761 (2022).
14. Lamy, F., Winckler, G., Arz, H. W., Farmer, J. R., Gottschalk, J., Lembke-Jene, L., ... & Zhao, X. Five million years of Antarctic Circumpolar Current strength variability. *Nature* **627**, 789-796 (2024).
15. Sprenk, D., Weber, M. E., Kuhn, G., Rosén, P., Frank, M., Molina-Kescher, M., ... & Röhling, H. G. Southern Ocean bioproductivity during the last glacial cycle–new detection method and decadal-scale insight from the Scotia Sea. *Geological Society, London, Special Publications* **381**, 245-261 (2013).
16. Wilson, D. J., Bertram, R. A., Needham, E. F., van de Flierdt, T., Welsh, K. J., McKay, R. M., ... & Escutia, C. Ice loss from the East Antarctic Ice Sheet during late Pleistocene interglacials. *Nature* **561**, 383-386 (2018).
17. Crotti, I., Quiquet, A., Landais, A., Stenni, B., Wilson, D., Severi, M., ... & Frezzotti, M. A refined age model and $^{143}Nd/^{144}Nd$ for the U1361A marine sediment core. *PANGAEA*, https://doi.org/10.1594/PANGAEA.941897 (2022).
18. Ai, X. E., Studer, A. S., Sigman, D. M., Martínez-García, A., Fripiat, F., Thöle, L. M. et al. Southern Ocean upwelling, Earth's obliquity, and glacial-interglacial atmospheric CO_2 change. *Science* **370**, 1348-1352 (2020).

19. Nürnberg, C. C., Bohrmann, G., Schlüter, M., & Frank, M. Barium accumulation in the Atlantic sector of the Southern Ocean: Results from 190,000-year records. *Paleoceanography* **12**, 594-603 (1997).

20. Crosta, X., Sturm, A., Armand, L., & Pichon, J. J. Late Quaternary sea ice history in the Indian sector of the Southern Ocean as recorded by diatom assemblages. *Mar. Micropaleontol.* **50**, 209-223 (2004).

21. Abelmann, A., Gersonde, R., Cortese, G., Kuhn, G., & Smetacek, V. Extensive phytoplankton blooms in the Atlantic sector of the glacial Southern Ocean. *Paleoceanography* **21** (2006).

22. Jaccard, S. L., Haug, G. H., Sigman, D. M., Pedersen, T. F., Thierstein, H. R., & Rohl, U. Glacial/interglacial changes in subarctic North Pacific stratification. *Science* **308**, 1003-1006 (2005).

23. Jaccard, S. L., Galbraith, E. D., Sigman, D. M., & Haug, G. H. A pervasive link between Antarctic ice core and subarctic Pacific sediment records over the past 800 kyrs. *Quat. Sci. Rev.* **29**, 206-212 (2010).

24. McDonald, D., Pedersen, T. F., & Crusius, J. Multiple late Quaternary episodes of exceptional diatom production in the Gulf of Alaska. *Deep-Sea Res. P.T.II* **46**, 2993-3017 (1999).

25. Costa, K. M., McManus, J. F., & Anderson, R. F. Paleoproductivity and Stratification across the Subarctic Pacific over Glacial-Interglacial Cycles. *Paleoceanogr. Paleoclimatol* **33**, 914-933 (2018).

26. Brunelle, B. G., Sigman, D. M., Cook, M. S., Keigwin, L. D., Haug, G. H., Plessen, B., ... & Jaccard, S. L. Evidence from diatom-bound nitrogen isotopes for subarctic Pacific stratification during the last ice age and a link to North Pacific denitrification changes. *Paleoceanography*, *22*(1) (2007).

27. Shigemitsu, M., Narita, H., Watanabe, Y. W., Harada, N., & Tsunogai, S. Ba, Si, U, Al, Sc, La, Th, C and $^{13}C/^{12}C$ in a sediment core in the western subarctic Pacific as proxies of past biological production. *Mar. Chem.* **106**, 442-455 (2007).

28. Fukuma, K., Harada, N. Paleointensity stratigraphy of North Pacific sediments. *Rep. Jpn. Mar. Sci. Technol. Cent*. **43**, 83-91 (2001).

29. Costa, K. M., McManus, J. F., Boulahanis, B., Carbotte, S. M., Winckler, G., Huybers, P. J., & Langmuir, C. H. Sedimentation, stratigraphy and physical properties of sediment on the Juan de Fuca Ridge. *Mar. Geol.* **380**, 163-173 (2016).